Journal of Controlled Release 262 (2017) 47–57

Contents lists available at ScienceDirect

Journal of Controlled Release

journal homepage: www.elsevier.com/locate/jconrel

A systematic comparison of clinically viable nanomedicines targeting HMG-CoA reductase in inflammatory atherosclerosis

Amr Alaarg[a,b,c], Max L. Senders[b,d], Aida Varela-Moreira[c,e], Carlos Pérez-Medina[b], Yiming Zhao[b], Jun Tang[f], Francois Fay[b,g], Thomas Reiner[f,h], Zahi A. Fayad[b], Wim E. Hennink[c], Josbert M. Metselaar[a,i], Willem J.M. Mulder[b,d,*], Gert Storm[a,c,j,**]

[a] Department of Biomaterials Science and Technology, MIRA Institute for Biomedical Technology and Technical Medicine, University of Twente, Enschede 7500 AE, The Netherlands
[b] Translational and Molecular Imaging Institute, Icahn School of Medicine at Mount Sinai, New York, NY 10029, USA
[c] Department of Pharmaceutics, Utrecht Institute for Pharmaceutical Sciences, Utrecht University, Utrecht 3584 CG, The Netherlands
[d] Department of Medical Biochemistry, Academic Medical Center, 1105 AZ Amsterdam, The Netherlands
[e] Department of Clinical Chemistry and Haematology, University Medical Centre Utrecht, Utrecht 3584 CX, The Netherlands
[f] Department of Radiology, Memorial Sloan Kettering Cancer Center, New York, NY 10065, USA
[g] Department of Chemistry, York College of The City University of New York, New York, NY 11451, USA
[h] Department of Radiology, Weill Cornell Medical College, New York, NY 10065, USA
[i] Department of Experimental Molecular Imaging, University Clinic and Helmholtz Institute for Biomedical Engineering, RWTH Aachen University, Aachen 52074, Germany
[j] Imaging Division, University Medical Centre Utrecht, Utrecht 3584 CX, The Netherlands

ARTICLE INFO

Keywords:
Atherosclerosis
Inflammation
Targeted drug delivery
Statins
Nanomedicine
Liposomes
Polymers
High-density lipoprotein
Macrophages

ABSTRACT

Atherosclerosis is a leading cause of worldwide morbidity and mortality whose management could benefit from novel targeted therapeutics. Nanoparticles are emerging as targeted drug delivery systems in chronic inflammatory disorders. To optimally exploit nanomedicines, understanding their biological behavior is crucial for further development of clinically relevant and efficacious nanotherapeutics intended to reduce plaque inflammation. Here, three clinically relevant nanomedicines, i.e., high-density lipoprotein ([S]-HDL), polymeric micelles ([S]-PM), and liposomes ([S]-LIP), that are loaded with the HMG-CoA reductase inhibitor simvastatin [S], were evaluated in the apolipoprotein *E*-deficient (*Apoe*$^{-/-}$) mouse model of atherosclerosis. We systematically employed quantitative techniques, including in vivo positron emission tomography imaging, gamma counting, and flow cytometry to evaluate the biodistribution, nanomedicines' uptake by plaque-associated macrophages/monocytes, and their efficacy to reduce macrophage burden in atherosclerotic plaques. The three formulations demonstrated distinct biological behavior in *Apoe*$^{-/-}$ mice. While [S]-PM and [S]-LIP possessed longer circulation half-lives, the three platforms accumulated to similar levels in atherosclerotic plaques. Moreover, [S]-HDL and [S]-PM showed higher uptake by plaque macrophages in comparison to [S]-LIP, while [S]-PM demonstrated the highest uptake by Ly6C^{high} monocytes. Among the three formulations, [S]-PM displayed the highest efficacy in reducing macrophage burden in advanced atherosclerotic plaques. In conclusion, our data demonstrate that [S]-PM is a promising targeted drug delivery system, which can be advanced for the treatment of atherosclerosis and other inflammatory disorders in the clinical settings. Our results also emphasize the importance of a thorough understanding of nanomedicines' biological performance, ranging from the whole body to the target cells, as well drug retention in the nanoparticles. Such systematic investigations would allow rational applications of nanomaterials', beyond cancer, facilitating the expansion of the nanomedicine horizon.

1. Introduction

Atherosclerosis is a chronic, systemic inflammatory disease of the large and medium-sized arteries, which can lead to life-threating events such as myocardial infarction and stroke [1]. According to the World Health Organization, 17.5 million deaths per year, an estimated 31% of

* Correspondence to: Willem J.M. Mulder, Translational and Molecular Imaging Institute, Icahn School of Medicine at Mount Sinai, New York, NY 10029, USA.
** Correspondence to: Gert Storm, Department of Pharmaceutics, Utrecht Institute for Pharmaceutical Sciences, Utrecht University, Utrecht 3584 CG, The Netherlands.
E-mail addresses: willem.mulder@mssm.edu (W.J.M. Mulder), G.Storm@uu.nl (G. Storm).

http://dx.doi.org/10.1016/j.jconrel.2017.07.013
Received 29 March 2017; Received in revised form 27 June 2017; Accepted 7 July 2017
Available online 09 July 2017

all deaths worldwide, can be attributed to atherosclerotic cardiovascular diseases [2]. The initiation and progression of atherosclerotic lesions are currently understood to have a central inflammatory component in which immune cells, including inflammatory monocytes and macrophages, play key roles [3,4]. At early stages, elevated levels of circulating apolipoprotein B-containing lipoproteins induce focal expression of endothelial adhesion molecules [5], which promote the recruitment of inflammatory Ly6C^{high} monocytes to the arterial wall [6]. Once adhered, monocytes transmigrate into the subendothelial space and differentiate into resident macrophages [4]. The continued accumulation of lipoproteins and immune cells, including macrophages, accelerates the development of focal lesions known as atherosclerotic plaques [7]. In advanced atherosclerosis, plaque-associated macrophages proliferate and secrete proinflammatory mediators, reactive oxygen species, and proteases which destabilize the plaque and aggravate the disease [8,9]. Additionally, recent preclinical [10] and clinical [11] work have identified cardiovascular events as key contributors to the aggravation of plaque inflammation, increasing secondary event's risk [12]. Thus, silencing plaque inflammation by targeting monocyte/macrophage burden is a compelling disease management strategy.

Over the last few decades, extensive research has been conducted to explore the potential use of nanomaterials as novel drug delivery systems in cancer [13–17] and other inflammatory disorders [18,19]. While liposomes [20] have always been frontrunners, the nanomedicine field has also witnessed an exponential increase in the number of new nanomaterials [21,22], including polymeric micelles [23,24] and high-density lipoproteins (HDL) [25] as systems which have already matured up to the level of clinical application [23,26,27]. However, the majority of studies explore and focus on only one specific nanomaterial, mainly for tumor targeting [28], without comparing performance against other existing nanocarriers. Beyond cancer, more comprehensive investigations of these nanomaterials, covering drug-nanocarrier compatibility (i.e., loading efficiency, and drug retention and release) and *in vivo* performance (i.e., pharmacokinetics, tissue distribution, atherosclerotic plaque targeting and efficacy), are necessary. Understanding the factors that govern nanomedicines' *in vivo* performance is critical to ensure rational optimization, adequate quality control, and potential early stage clinical translation [29,30].

3-Hydroxy-3-methylglutaryl coenzyme A reductase (HMG-CoA) inhibitors, also known as statins, are the standard of care for patients with atherosclerotic cardiovascular diseases. Their oral application leads to reduced low-density lipoprotein (LDL) cholesterol blood levels, primarily by modulating hepatic LDL receptor expression [31]. Also, HMG-CoA inhibitors display pleiotropic effects at high doses, including anti-inflammatory and anti-proliferative activities [32,33]. In a clinical trial, high dose oral statin therapy was shown to reduce atherosclerotic inflammation, using ^{18}F-fluorodeoxyglucose-positron emission tomography/computed tomographic imaging (FDG-PET/CT) in patients [34]. Moreover, in an atherosclerotic mouse model, Sparrow et al. showed that oral simvastatin, a frequently used HMG-CoA inhibitor, has anti-inflammatory and anti-atherosclerotic effects at a dose of 100 mg/kg, independent of its cholesterol-lowering properties [35]. However, increasing the oral statin standard dose in human is not possible because of the dose-dependent adverse effects such as myopathy and hepatoxicity [36]. At the same time, orally administered statins undergo hepatic metabolism, which results in a very poor plaque bioavailibility [37]. Therefore, intravenous nanocarrier-mediated targeting of HMG-CoA inhibitors to atherosclerotic plaques is an attractive approach to achieve enhanced anti-inflammatory and anti-atherosclerotic effects, as we have shown for simvastatin-loaded HDL ([S]-HDL) [38,39].

In this paper, we present a comprehensive comparative analysis of three established and clinically viable nanomedicines targeting the HMG-CoA inhibitor simvastatin [S] to atherosclerotic plaques. The nanomedicines include [S]-HDL, [S]-*N*-(2-hydroxypropyl)-methacrylamide benzyl mPEG-*b*-p(HPMAm-Bz)-based PEGylated polymeric micelles (mPEG-*b*-p(HPMAm-Bz); [S]-PM), and [S]-PEGylated liposomes ([S]-LIP) (Fig. 1). We aimed to systematically investigate and compare the performance of the three [S]-nanomedicines in *Apoe*$^{-/-}$ mice with advanced atherosclerosis. To enable this, we implemented a quantitative and comparative approach, combining sensitive techniques, including *in vivo* positron emission tomography (PET), gamma counting, and multicolor flow cytometry, acquiring critical performance parameters of these three distinct nanomedicine platforms. The head-to-head comparison disclosed marked differences between the platforms, underscoring the significance of using quantitative and sensitive techniques, such as PET and flow cytometry, to relate organ distribution and immune cell specificity to nanomedicines' efficacy.

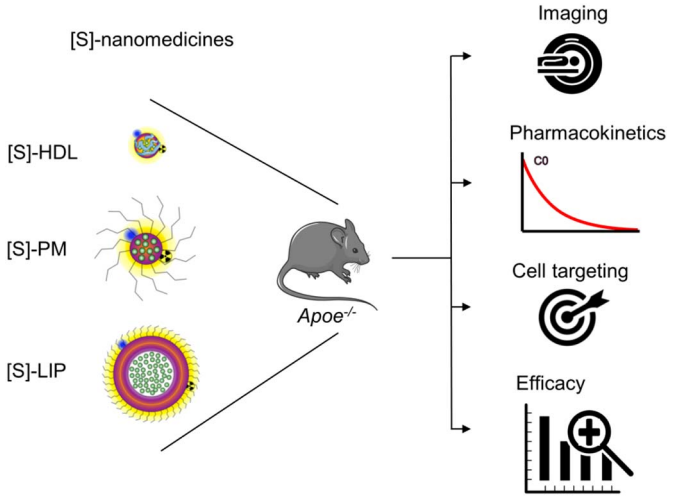

Fig. 1. Schematic of the [S]-nanomedicines and study design. [S]-HDL, [S]-PM, and [S]-LIP were evaluated in *Apoe*$^{-/-}$ mice with advanced atherosclerosis. To attain a thorough understanding of the *in vivo* behavior of the three platforms, we dual-labeled them with Zirconium-89 (^{89}Zr) and the near-infrared dye Cy5.5. The ^{89}Zr signal was exploited to provide a sensitive and quantitative assessment of their biodistribution and pharmacokinetics using noninvasive PET/CT imaging and gamma counting. The Cy5.5 signal was used to evaluate immune cell targeting in atherosclerotic plaques, blood, and spleen using flow cytometry. The efficacy of the three [S]-nanomedicines in *Apoe*$^{-/-}$ was quantitatively assessed by flow cytometry. [S]: simvastatin; HDL: high density lipoprotein; PM: polymeric micelles; LIP: liposomes; *Apoe*$^{-/-}$: apolipoprotein *E*-deficient.

2. Materials and methods

2.1. Materials and radiochemistry

1,2-Dipalmitoyl-*sn*-glycero-3-phosphocholine (DPPC), *N*-(carbonyl-methoxy-PEG2000)-1,2-distearoyl-*sn*-glycero-3-phosphoethanolamine (DSPE-PEG2000), cholesterol, 1-myristoyl-2-hydroxy-*sn*-glycerophosphocholine (MHPC), and 1,2-dimyristoyl-*sn*-glycero-3-phosphatidylcholine (DMPC) were purchased from Avanti Polar Lipids. The copolymers (methoxy poly(ethylene glycol)-*b*-(*N*-(2-benzoyloxypropyl) methacrylamide)) (mPEG-*b*-p(HPMAm-Bz)) and the amino-functionalized version, mPEG-*b*-p(HPMA-Bz-co-AEMAm), were synthesized by free radical polymerization, using mPEG$_2$-ABCPA as macroinitiator and HPMA-Bz as a monomer, as previously reported [40]. Briefly, the monomer and the macroinitiator were dissolved at a molar ratio of 200:1 in dried (over 4 Å molecular sieves) acetonitrile (Biosolve Ltd) at a final concentration of 300 mg/mL. The solution was flushed with nitrogen gas for 30 min and then immersed in a silicone bath at 70 °C for at least 17 h. Afterward, the solution was placed in cold diethyl ether to precipitate the formed polymer and centrifuged at 2600 × *g* for 15 min. The supernatant was discarded, and the pellet was re-dissolved in acetonitrile. This procedure was repeated three times, and the final product was dried under vacuum overnight at room temperature (RT) to remove the remaining organic solvent. For the synthesis of the

amine-functionalized copolymer, 2% (moles) of AEMAm, *N*-(2-aminoethyl) methacrylamide hydrochloride, (relative to HPMA-Bz) was added to the reaction mixture and the reaction was conducted as described above. DSPE-Cyanine5.5 (Cy5.5) was purchased from SyMO-Chem BV while synthesis and Cy5.5 labeling of mPEG-*b*-p(HPMAm-Bz) were done according to a method reported before [40]. Simvastatin and simvastatin sodium salt were obtained from AK Scientific and Cayman Chemical, respectively. All other materials were purchased from Sigma-Aldrich unless otherwise stated.

Zirconium-89 (^{89}Zr) was produced at Memorial Sloan Kettering Cancer Center on a TR19/9 variable-beam energy cyclotron (Ebco Industries Inc.) via the ^{89}Y(p,n) ^{89}Zr reaction and purified in accordance with the previously reported method [41]. Activity was measured using a CRC 15R dose calibrator (Capintec).

2.2. Characterization of mPEG-b-p(HPMA-Bz) copolymer

Gel Permeation Chromatography (GPC) was performed to determine the number average molecular weight (M_n), weight average molecular weight (M_w) and polydispersity (M_w/M_n) of the synthesized polymers. Two serial PLgel 5 μm MIXED-D columns (Polymer Laboratories) were used, and the run was performed in 10 mM LiCl DMF, at a flow rate of 1 mL/min and a column temperature of 65 °C. PEGs of narrow molecular weight distribution were used as standards. Samples were prepared at a concentration of 5 mg/mL in 10 mM LiCl DMF and allowed to dissolve for 30 min at 37 °C.

^{1}H NMR spectrum of mPEG-b-p(HPMAm-Bz) was recorded using a Gemini 300 MHz spectrometer (Varian Associates Inc. NMR Instruments), using DMSO-d_6 as a solvent and the DMSO peak at 2.50 ppm as a reference. Chemical shifts of PEG-HPMA-Bz were assigned as described elsewhere [40]. The ratio between HPMA-Bz and mPEG was determined by the integral value of aromatic protons of HPMA-Bz (8.0 ppm, 2H, aromatic CH) divided by two, and the integral value of the methylene protons of mPEG (3.40–3.60 ppm, 448H, O-CH_2-CH_2) divided by 448 (average number of protons per PEG chain, M_n = 5000 g/mol). The average number molecular weight (M_n) of the block copolymer was determined as follows:

$$\mathrm{Mn} = \frac{(\text{integral at 8.0 ppm}) \times \text{molar mass of HMPA} - \mathrm{Bz}}{\text{integral at 3.40–3.60 ppm}/448} + 5000\ \mathrm{g}\Big/\mathrm{mol}$$

The copolymers used to prepare the [S]-PM, i.e. mPEG-*b*-p(HPMAm-Bz) and the amine-functionalized, mPEG-*b*-p(HPMA-Bzco-AEMAm), were synthesized by free radical polymerization via a macroinitiator route [40]. Both copolymers show similar number-average molecular weight (Mn) ~22 KDa and PDI ~1.7 based on GPC and ^{1}H NMR analyses (Supporting Figs. 1 and 2 and Supporting Table 1).

2.3. Assessment of simvastatin and simvastatin sodium salt activity

To assure that both simvastatin, used in [S]-HDL and [S]-PM, and simvastatin sodium salt, used in [S]-LIP, have equipotent pharmacological activity, we assessed their dose-dependent effects on macrophage proliferation in vitro. RAW264.7 macrophages, obtained from ATCC, were cultured in Dulbecco's Modified Eagle's Medium (DMEM) high glucose (Corning) supplemented with 10% (v/v) fetal bovine serum, penicillin (100 IU/mL), streptomycin (100 μg/mL), and amphotericin B (0.25 μg/mL), and incubated at 37 °C under a 5% CO_2 atmosphere. Cells were seeded at a density of 5000 cells per well in a 96-well plate. After 24 h, cells were treated with simvastatin or simvastatin sodium salt at the indicated concentrations for 24 h. To determine the number of proliferating cells, bromodeoxyuridine (BrdU) reagent was added to the cells for 4 h, and an ELISA BrdU colorimetric immunoassay (Hoffman-La Roche Ltd) was performed, according to the manufacturer's protocol. The BrdU assay showed that both forms of simvastatin possess comparable dose-dependent inhibitory effects on macrophage proliferation (Supporting Fig. 3).

2.4. Formulation of simvastatin nanomedicines

Formulation of the HMG-CoA inhibitor simvastatin HDL ([S]-HDL) was done according to a method reported before [38,39]. In brief, simvastatin, DMPC, and MHPC, in a weight % ratio of 14:78:8, respectively, were dissolved in a chloroform/methanol mixture (4:1 by volume) and a lipid film was prepared by rotary evaporation (Büchi Labortechnik) and dried under a nitrogen stream for 1 h until complete dryness. The lipid film was then hydrated with human apolipoprotein A1 (APOA1, isolated from human plasma) in PBS (APOA1 and phospholipids in a 1:9 weight ratio). The mixture was incubated at 37 °C until the film was completely hydrated. The lipid dispersion was subjected to ultrasonication to form [S]-HDL nanomedicine formulation.

To formulate HMG-CoA inhibitor liposomes ([S]-LIP), we used simvastatin provided as sodium salt, a water-soluble derivative that allows its entrapment in liposomes. Liposome preparation was modified from a method described previously [42]. Briefly, DPPC, cholesterol, and DSPE-PEG2000, in a weight % ratio of 61.7:33.3:5, respectively, were dissolved a chloroform/methanol mixture (4:1 by volume) in a round-bottom flask. A lipid film was prepared by evaporation of the solvents and subsequently hydrated with a solution of 5 mg/mL simvastatin (sodium salt) in PBS (5 mL). The mixture was then heated at 60 °C until the film was completely hydrated. To downsize the lipid dispersion, the lipid particles were subjected to multiple extrusion steps through polycarbonate membranes (Whatman, Nuclepore) with a final pore size of 100 nm using a Lipex extruder (Northern Lipids).

Preparation of HMG-CoA inhibitor HPMA-based polymeric micelles ([S]-PM) was done as described by Shi et al. [40]. Briefly, mPEG-*b*-p(HPMAm-Bz) copolymer (10 mg) and simvastatin (2 mg) were both completely dissolved in 0.5 mL tetrahydrofuran (THF). Then the polymer/drug mixture was slowly added dropwise to 2 mL of Milli-Q water while stirring to form [S]-PM. The mixture was then incubated for 48 h at RT to allow evaporation of THF.

[S]-HDL was washed with PBS at least three times using ultrafiltration units with a 50 kDa molecular weight cutoff (MWCO) (Sartorius Stedim Biotech SA). [S]-PM or [S]-LIP were purified with PBS using VivaFlow crossflow cassettes filtration units with a 100 kDa MWCO (Sartorius Stedim Biotech SA). All the three formulations were centrifuged at 4000 × *g* for 30 min to remove any aggregates. Finally, each formulation was filtered through a 0.22 μm nylon membrane filter (CellTreat Scientific Products).

2.5. Dual labeling of simvastatin nanomedicines

The [S]-nanomedicines were labeled with Cy5.5 to allow near-infrared fluorescence (NIRF) imaging and flow cytometry studies. Briefly, 0.5% of DSPE-Cy5.5 was incorporated into the lipid film of either [S]-HDL or [S]-LIP during the lipid film formation (modified from [43]). For [S]-PM, 0.5% of Cy5.5-labeled mPEG-*b*-p(HPMAm-Bz) was added to the simvastatin/polymer mixture in THF before adding to Milli-Q water (modified from Shi et al. [40]).

To additionally label the nanomedicines with ^{89}Zr for PET imaging and quantitative biodistribution assessment, a similar approach was followed as we previously reported [41,44]. Briefly, 0.5% of DSPE-desferrioxamine (DSPE-DFO) [41] was incorporated in the lipid film of [S]-HDL or [S]-LIP. For the polymeric micelles, to functionalize the polymer with DFO, a solution of the amine-functionalized copolymer mPEG-*b*-p(HPMA-Bz-co-AEMAm) (2.0 mg), *p*-isothiocyanatobenzyl-DFO (Macrocyclics) (40 μg, ~1 eq) and *N*,*N*-diisopropylethylamine (1.0 μL) in dimethylsulfoxide (0.21 mL) was heated at 40 °C for 8 h. The mixture was then allowed to cool down to RT. Water (1.8 mL) was added, and the resulting milky solution was concentrated by centrifugal filtration using a 10 kDa MWCO tube and washed three times with Milli-Q water (2 mL). The final retentate was dried under vacuum to

yield the DFO-modified polymer as a white solid (2.0 mg). The DFO-modified mPEG-b-p(HPMAm-Bz) was added at 5% of the total polymer weight to the formulation mix at the expense of non-modified mPEG-b-p(HPMAm-Bz). Subsequently, a PBS dispersion of the corresponding DFO-bearing nanomedicine formulation was reacted with [^{89}Zr]$Zr_2(C_2O_4)_2$ at pH 7.1–7.4 for 1 h at 37 °C. The dispersion was allowed to cool down to RT, and the radiolabeled nanocarriers were purified by centrifugal filtration using 10 kDa MWCO filter tubes for [S]-HDL, and 100 kDa MWCO filter tubes for [S]-LIP and [S]-PM. The radiochemical yield was ≥80% with radiochemical purities > 95% for the three formulations.

2.6. Characterization

The mean particle size and polydispersity index (PDI) of the different [S]-nanomedicines used in this study were determined by dynamic light scattering using a Malvern NanoSeries *Z*-Sizer. The Zeta (ζ)-potential was determined using a PALS analyzer (Brookhaven Instruments Corp.) where [S]-nanomedicine samples were diluted in 10 mM HEPES buffer (pH 7.4) before measurements. The morphology of the nanomedicines was determined by transition emission microscopy (TEM). Briefly, the original PBS solvent was replaced by an ammonium acetate buffer and then mixed with 2% (wt/vol) sodium phosphotungstate (pH = 7.4) to negatively stain the [S]-nanomedicine. The solution was then cast dried on a nickel grid and imaged with a Hitachi H7650 TEM.

2.7. HPLC and radio-HPLC

Simvastatin concentrations in the different samples were determined as previously reported [38]. The simvastatin content of the nanocarriers or samples from drug release studies (described in the following section) was determined by HPLC, using a Prominence LC-20AB system (Shimadzu) equipped with a C18 column at a flow rate of 0.5 mL/min, utilizing an isocratic mobile phase composed of 80% acetonitrile, 20% H_2O, and 0.1% trifluoroacetic acid. Simvastatin was detected at a wavelength of 238 nm using SPD-M10AVP photodiode array detector.

Radio-HPLC was performed using a similar Shimadzu system additionally equipped with a Lablogic Scan-RAM Radio-TLC/HPLC detector. Size-exclusion chromatography was performed on a Superdex 10/300 column (GE Healthcare Life Sciences) using PBS as eluent at a flow rate of 1 mL/min.

2.8. Drug release in serum

The release of simvastatin from the nanocarriers was studied as described previously [45,46], with some slight modifications. Briefly, 0.1 mL of [S]-HDL, [S]-PM, or [S]-LIP (1 mg/mL simvastatin), was mixed with 0.9 mL fetal bovine serum (FBS) and samples were incubated at 37 °C for 1, 2, 4, 8, and 24 h. At these time points, samples were subjected to size-exclusion high-performance liquid chromatography (SEC) for nanocarrier-protein separation and fractionation using a Prominence LC-20AB HPLC system (Shimadzu) equipped with a fraction collector, FRC-10A (Shimadzu) and a Superose 6 10/300 GL Fast protein liquid chromatography column (GE Healthcare Life Sciences). PBS was used as eluent at a flow rate of 0.6 mL/min. The nanocarrier fractions (containing simvastatin retained in the nanocarrier) and serum fractions (protein-associated simvastatin) were collected, and their corresponding simvastatin content was extracted with acetonitrile and analyzed by HPLC as detailed above.

2.9. Animals and treatment procedure

Female *Apoe*$^{-/-}$ mice (B6.129P2-Apoetm1Unc/J, 6 weeks old) were purchased from The Jackson Laboratory and were fed a high-fat diet (HFD) (Harlan Teklad TD.88137, 42% calories from fat) for 18 weeks (average weight: 27.5 ± 3.3 g). Under these conditions, the animals develop atherosclerotic lesions because of the high LDL cholesterol concentrations in the blood resulting from the lack of apolipoprotein E [47]. All animal experiments were performed in accordance with protocols approved by the Institutional Animal Care and User Committees of Mount Sinai and Memorial Sloan Kettering Cancer Center. All experiments adhered to National Institutes of Health guidelines for animal welfare. All animals were injected intravenously with the corresponding nanomedicines in a 150–200 μL of PBS solution via the lateral tail vein.

2.10. Micro-PET/CT imaging

Twenty four hours after injecting the ^{89}Zr-[S]-nanomedicines (0.18 ± 0.03 mCi/animal), the animals (n = 3 per treatment type) were anesthetized with a mixture of isoflurane (Baxter Healthcare) and oxygen gas (2% for induction and 1% for maintenance), and scans were then obtained using an Inveon PET/CT scanner (Siemens Healthcare Global). Whole-body PET static scans recording a minimum of 50 million coincident events were performed with duration of 10–20 min. Whole body standard low-magnification CT scans were obtained with the x-ray tube set at a voltage of 80 kV and current of 500 mA. The CT scan was acquired using 120 rotational steps for a total of 220°, yielding an estimated scan time of 120 s with an exposure of 145 ms/frame. The counting rates in the reconstructed images were converted to activity concentrations (%ID/g) by use of a system calibration factor derived from the imaging of a mouse-sized water-equivalent phantom containing the radionuclide. Images were analyzed using Inveon Research Workplace software (Siemens Healthcare Global). Activity concentration was quantified by averaging the maximum values in at least 5 ROIs drawn on adjacent slices of the tissue of interest.

2.11. Pharmacokinetics and biodistribution

Apoe$^{-/-}$ mice (n ≥ 3 per [S]-nanomedicine type) were administered 26 ± 5 μCi ^{89}Zr/animal of the corresponding dual labeled ^{89}Zr/Cy5.5 [S]-nanomedicines at doses of 0.8 mg Cy5.5/kg and 60 mg simvastatin/kg (as in the therapeutic study). Blood was sampled (~ 10–20 μL/each sample) at predetermined time points (30 min, 1, 2, 4, 8, and 24 h) after injection. After 24 h, the mice were euthanized and perfused with 30 mL PBS/mouse through cardiac puncture, and organs of interest (aorta, liver, spleen, kidneys, lungs, heart, and brain) were excised. The blood samples (at the different time points) and samples of other tissues were weighed, and their radioactivity content was quantified using Wizard 2470 Automatic Gamma Counter (Perkin Elmer). The values were corrected for ^{89}Zr decay and radioactivity concentration was calculated as a percentage of injected dose per gram of tissue (%ID/g).

[S]-nanomedicines biodistribution was also qualitatively assessed by NIRF imaging and autoradiography. Perfused tissue samples were placed on a thick black paper and imaged on a Xenogen IVIS Spectrum Preclinical Imaging System (Perkin Elmer). Fluorescence images were acquired with selected excitation and emission band-pass filters: for Cy5.5 λ_{Exc} = 640 ± 18 nm, λ_{Em} = 720 ± 10 nm. Exposure time for each image was 2 s. To assess the radiotracer distribution, tissues were placed on a film cassette against a phosphorimaging plate (BASMSM-2325, Fujifilm) for either 24 h (aortas) or 18 h (all other organs) at − 20 °C. The plates were then read at a pixel resolution of 25 μm in a Typhoon 7000IP plate reader (GE Healthcare).

2.12. Flow cytometry

To study the uptake of [S]-nanomedicines by immune cells, we used flow cytometry protocols similar to what was previously reported [38,47]. Briefly, *Apoe*$^{-/-}$ mice (n = 4 per group, 18 weeks on HFD)

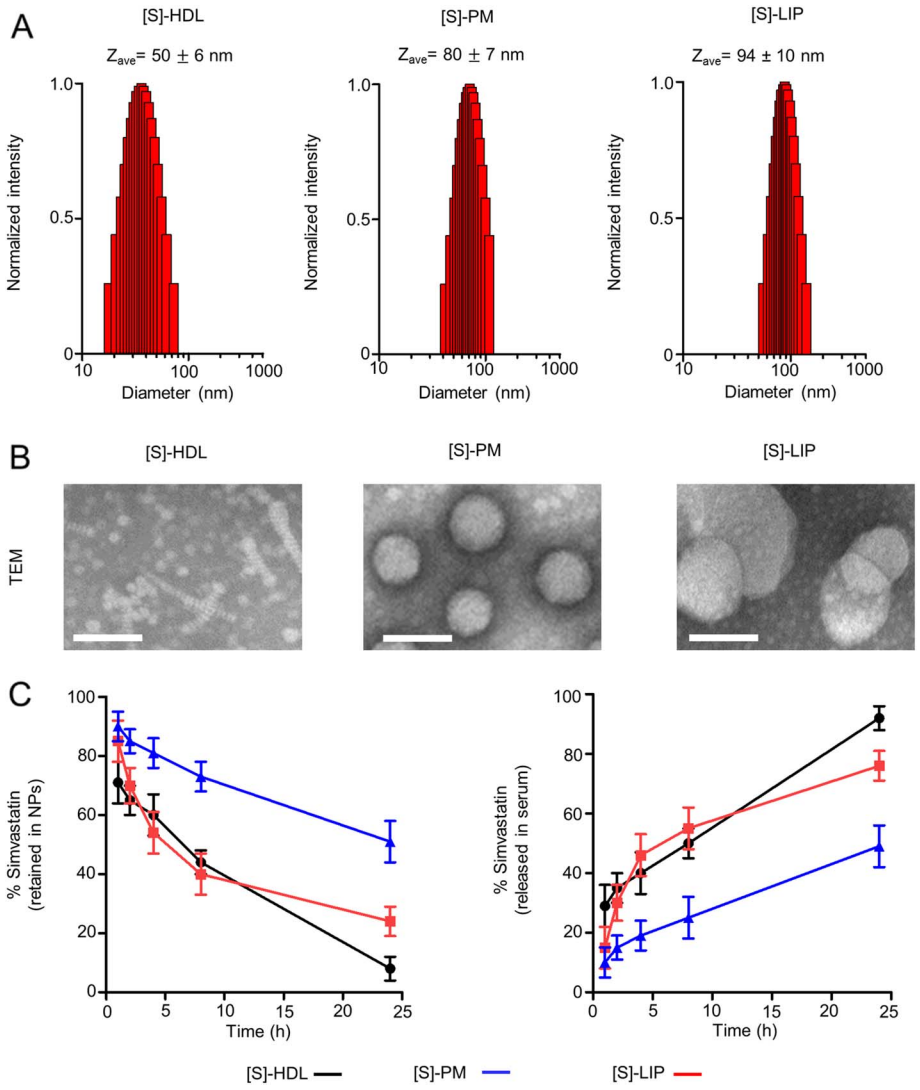

Fig. 2. Characterization and drug release kinetics of the [S]-nanomedicines. (A) Particle size distribution of [S]-HDL, [S]-PM, and [S]-LIP was evaluated by dynamic light scattering. (B) Negative staining TEM images of the aforementioned nanomedicines. Scale bar = 100 nm. (C) The release of simvastatin from the three nanomedicines in fetal bovine serum (FBS) was assessed using size-exclusion chromatography and high-performance liquid chromatography (HPLC) as described in Supporting Fig. 3. [S]: simvastatin; HDL: high density lipoprotein; PM: polymeric micelles; LIP: liposomes; TEM: transmission electron microscopy; NPs: nanoparticles; h: hours; nm: nanometer.

were injected with Cy5.5-labeled [S]-nanomedicines at 0.8 mg Cy5.5/kg (at a dose of 60 mg/kg simvastatin). After 24 h, to prepare cells for flow cytometry, blood was collected by cardiac puncture into tubes with a 50 mM EDTA solution as an anticoagulant. Red blood cells (RBCs) were lysed using RBC lysis buffer (BD Biosciences). Afterward, animals were perfused with 30 mL PBS/mouse. The whole aorta, from the aortic root to the iliac bifurcation, and spleen were harvested. Single-cell suspensions were obtained as follows: aortas were diced and digested with a cocktail of enzymes, including 4.5 U/mL liberase TH (Roche), 60 U/mL hyaluronidase (Sigma-Aldrich), and 40 U/mL DNase (Sigma-Aldrich), in a 37 °C oven for 1 h while shaking. Then, tissue aggregates, extracellular matrix, and cell debris were removed by filtration. Spleens were also diced, and RBCs were removed using the same lysis buffer described above. To identify macrophages, monocytes, dendritic cells, neutrophils, and other immune cells, a cocktail of antibodies was used (antibodies, clones, and suppliers shown in Table S.2). Cy5.5 signal was detected on the Alexa700 channel.

In the efficacy study, we quantified the number of macrophages and Ly6C^{high} monocytes in atherosclerotic plaques. Complete blood count was also performed to assess the number of immune cells in the blood. Mice (n = 8–10/group, 18 weeks on HFD) were administered the corresponding treatments ([S]-nanomedicines, 60 mg/kg simvastatin; PBS, or oral simvastatin, 60 mg/kg) once every 72 h for a week (three injections in total). Mice were sacrificed 24 h after the last injection, and immune cells from aorta and blood were isolated and quantified. For both the targeting study and the efficacy study, we adopted a strict flow cytometry protocol by running 'fluorescence minus one' (FMO) controls to precisely gate the right cell population. In an FMO control stain sample, all reagents used in a given multicolor sample are included except the reagent with which the exact cell population is to be determined. All samples were measured on an LSRII (BD Biosciences) flow cytometer, and results were analyzed with FlowJo (Tree Star) software.

Serum from animals in the efficacy study was subjected to a biochemical analysis (ALX Laboratories, NY) to determine typical blood biochemistry constituents, including cholesterol and triglycerides, and toxicity markers like alanine transaminase.

2.13. Statistical analysis

Statistical analysis was performed using Prism (GraphPad), and data are expressed as a mean ± standard error of the mean. Differences between groups were assessed by one-way analysis of variance (ANOVA) followed by a post hoc test (Bonferroni's test) for multiple comparisons. $^{*}P \leq 0.05$; $^{**}P \leq 0.01$; $^{***}P \leq 0.001$ A value of $P < 0.05$ was considered statistically significant.

3. Results and discussion

The aim of this study was to target HMG-CoA in atherosclerotic plaques by simvastatin-loaded nanomedicines and to understand the

parameters that control their *in vivo* performance. Liposomes were included as they are often regarded as the gold standard nanomedicine drug delivery system and were the first to make clinical translation [20,43]. Additionally, liposomes have been shown to successfully target atherosclerotic plaques in rabbits [43,48] and humans [49]. HDL, a natural self-assembled nanocarrier, has an intrinsic affinity to plaque macrophages in different atherosclerosis animal models [44,50]. The natural targeting ability of HDL and the possibility to incorporate hydrophobic compounds in its core makes it an attractive platform for drug delivery [51]. HPMA block copolymer-based micelles were shown to improve the retention of hydrophobic chemotherapeutic drugs in their matrix [52–54], offering effective targeted drug delivery to tumors and inflammatory sites [53,55,56]. However, they have not yet been evaluated in atherosclerosis. Here, we explored their ability to target atherosclerotic plaques for the first time and compared their performance with previously assessed HDL and liposomal formulations.

3.1. Preparation and characterization of simvastatin nanomedicines

[S]-HDL was prepared by ultrasonication, a well-established method to encapsulate hydrophobic drugs in HDL nanoparticles [57,58]. [S]-LIP was prepared using a more water-soluble derivative, i.e., simvastatin (sodium salt). [S]-PM was formulated by dropping a THF solution of the polymer and simvastatin into water followed by evaporation of THF, a method that was previously used to encapsulate hydrophobic drugs [52,59].

DLS analysis showed that the mean particle sizes (*Z*-average) of the three [S]-nanomedicines were different and none of them was larger than 100 nm. [S]-HDL possessed the smallest mean diameter (~50 nm) with a PDI ~ 0.22 (Fig. 2A and Table 1). Analysis of [S]-HDL by TEM showed the typical discoidal shape of HDL nanoparticles as reported before [38] (Fig. 2B). DLS analysis showed that [S]-PM and [S]-LIP had larger mean diameters of ~80 and ~95 nm, respectively (Fig. 2A and Table 1). Both formulations showed a low PDI ~ 0.1 (Table 1). TEM images of [S]-PM and [S]-LIP showed spherical particles (Fig. 2B). The zeta (ζ) potential of the three [S]-nanomedicines was negative in 10 mM HEPES buffer (pH 7.4), ranging from −5 mV for [S]-PM to ~ −15 mV for both the liposomal and HDL formulations (Table 1). All the three [S]-nanomedicines had high simvastatin entrapment efficiency (> 60%) as shown in Table 1.

3.2. Drug release kinetics in serum

The extent and rate of drug release while nanocarriers circulate in the bloodstream is an important factor which can strongly affect a drug-loaded nanocarrier's targeting efficiency and resulting therapeutic efficacy. The release kinetics of the three simvastatin nanoformulations in 90% serum at 37 °C, mimicking physiological conditions, was analyzed. Using size exclusion chromatography, we separated the nanocarrier from the serum proteins, and then analyzed the simvastatin content in each fraction (Supporting Fig. 4). The release kinetics of simvastatin from [S]-HDL was similar to that of [S]-LIP but much more rapid than [S]-PM (Fig. 2C). By the end of the 24 h incubation period, ~50% of the simvastatin from [S]-PM was released compared to ~80% and 90% in the case of [S]-LIP and [S]-HDL, respectively. The higher drug retention in case of [S]-PM can be explained by purposely designed physicochemical features that enhance hydrophobic and π-π stacking interactions [40,56]. In the case of [S]-LIP, simvastatin sodium salt was used to increase drug entrapment in the liposomal formulation. However, according to the manufacturer (Cayman), simvastatin (sodium salt) is sparingly soluble in aqueous solutions and probably also possess an affinity for the lipid bilayer, which may have resulted in drug leakage from the [S]-LIP upon interaction with serum proteins. Similarly, HDL has a dynamic structure, which could result in the exchange of lipid components upon interaction with other serum proteins, resulting in drug leakage [45].

Table 1
Characteristics of [S]-nanomedicines.

	[S]-HDL	[S]-PM	[S]-LIP
$Z_{ave.}$	50 ± 6 nm	80 ± 7 nm	94 ± 10 nm
PDI	0.22 ± 0.03	0.11 ± 0.01	0.10 ± 0.06
Zeta (ζ) potential (mV)	−15.8 ± 3.5	−5.1 ± 0.9	−15.1 ± 0.7
EE (%)	60 ± 7%	65 ± 8%	71 ± 3%

Data are presented as mean ± SD of three separately prepared batches of [S]-HDL, [S]-PM, or [S]-LIP. [S]: simvastatin; HDL: high density lipoprotein; PM: polymeric micelles; LIP: liposomes; Zave.: Z average; mV: millivolt; PDI; polydispersity index, EE; entrapment efficiency.

3.3. Dual labeling of simvastatin nanomedicines

To better understand [S]-nanomedicines' biodistribution and uptake by immune cells, we employed a dual-labeling strategy using ^{89}Zr as a radioactive tag detectable by PET and gamma counting, and Cy5.5 for NIRF imaging and flow cytometry. ^{89}Zr has a physical half-life of 78.4 h, making it suitable for long-circulating nanoparticles [41] and antibodies [60]. Additionally, PET imaging and gamma counting are sensitive, quantitative methods for evaluating [S]-nanomedicines' pharmacokinetics, whole-body, and organ biodistribution, while flow cytometry allows assessment of immune cell specificity in atherosclerotic plaques and other tissues in a quantitative fashion. Both labels (i.e. ^{89}Zr and Cy5.5) on [S]-HDL, [S]-PM, and [S]-LIP eluted at the same time on size-exclusion chromatography columns, indicative of proper label stability.

3.4. Pharmacokinetics, in vivo imaging and biodistribution

In vivo evaluation of the three [S]-nanomedicines started with an assessment of their circulation kinetics in *Apoe*$^{-/-}$ mice using gamma counting to quantify blood radioactivity levels over time (Fig. 3B). After 24 h, [S]-PM and [S]-LIP showed longer circulation times in blood in comparison with [S]-HDL (~10% ID/g remaining in blood vs ~1% ID/g for [S]-HDL). The longer circulation times for [S]-PM and [S]-LIP is likely related to their PEGylated surface and relatively large size as compared to [S]-HDL.

To study the tissue distribution of the [S]-nanomedicines non-invasively, we employed PET/CT imaging (Fig. 3C). PET imaging offers high sensitivity with deep tissue penetration [50,61]. At 24 h after injection, PET/CT imaging showed predominant accumulation in liver and spleen. This is in line with the dominant role of mononuclear phagocytic system (MPS) macrophages in the removal of intravenously administered nanosystems [62]. [S]-HDL showed a relatively high signal in the kidneys, in line with a previously reported [50,63,64] renal clearance of comparatively smaller nanoparticles. The total body signal detected in mice which received [S]-PM or [S]-LIP was higher than that of [S]-HDL, implying faster body clearance of the latter (Supporting Fig. 5).

We subsequently excised the tissues of interest from *Apoe*$^{-/-}$ mice and analyzed their radioactivity content 24 h after i.v. administration. *Ex vivo* analysis of the radioactivity distribution corroborated the observations from pharmacokinetic and PET imaging studies (Fig. 3D and E). [S]-PM and [S]-LIP showed the highest accumulation in spleen and liver, ~25–30% ID/g and 10–15% ID/g, respectively (Fig. 3D), while [S]-HDL showed relatively high kidney accumulation. These results were in line with the qualitative autoradiographic analysis (Fig. 3E) and NIRF imaging (Supporting Fig. 6).

3.5. Targeting to atherosclerotic plaques and lesion-associated macrophages and monocytes

We investigated the plaque targeting ability of the [S]-

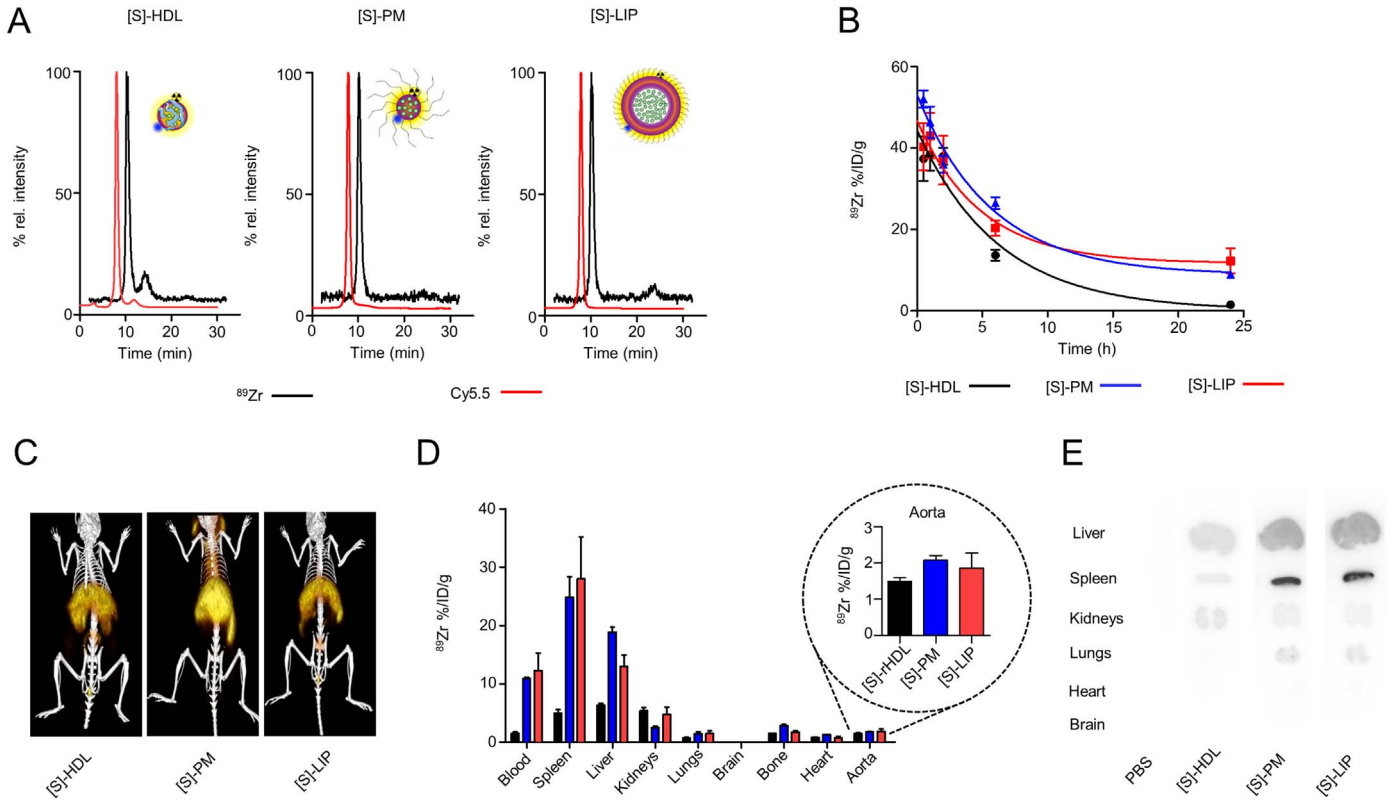

Fig. 3. Dual labeling of [S]-nanomedicines, and their pharmacokinetics and biodistribution evaluation in *Apoe*$^{-/-}$ mice with advanced atherosclerosis. (A) Size exclusion chromatograms showing coelution of Cy5.5 (λ = 675 nm, red trace) and ^{89}Zr (black, radioactive trace) on the corresponding nanomedicines (The radioactive trace was nudged by 5% to prevent visual overlapping). (B) Blood time-activity curves for the different ^{89}Zr-labeled [S]-nanomedicines, as determined by gamma counting ($n \geq 3$ per condition). (C) Three-dimensional rendering of PET/CT fusion images 24 h after injection ($n = 3$ per condition). (D) Quantitative assessment of radioactivity distribution in selected tissues using gamma counting 24 h after injection ($n \geq 3$ per condition). (E) Autoradiography of selected tissues 24 h after injection. [S]: simvastatin; HDL: high density lipoprotein; PM: polymeric micelles; LIP: liposomes; % rel. intensity: percentage relative intensity; ^{89}Zr: Zirconium-89; Cy5.5: Cyanine5.5; %ID/g: percentage injected dose per gram of tissue; min: minutes; h: hours. (For interpretation of the references to colour in this figure legend, the reader is referred to the web version of this article.)

nanomedicines *Apoe*$^{-/-}$ mice aortas. Interestingly, using gamma counting, the radioactivity concentrations in the excised aortas were similar for the three formulations (~1.5–2% ID/g) with no statistically significant differences (Fig. 3D, right). These findings are especially striking given the difference in blood circulation half-lives. We also evaluated regional distribution within the aorta using autoradiography and NIRF imaging for the three formulations (Fig. 4A). We found co-localization between radioactivity disposition and NIRF signal in the focal atherosclerotic lesions, especially in aortic roots, an area which is known to reproducibly develop atherosclerotic plaque [65–67].

Since macrophages and monocytes are the key immune cells that drive atherosclerosis progression [9], we sought to study the uptake of the three [S]-nanomedicine types by these key cells in aortic plaques of *Apoe*$^{-/-}$ mice with advanced atherosclerosis. We applied a flow cytometry protocol and gating procedures adapted from previous studies [8,47] (Fig. 4B). After 24 h i.v. administration, the aortas were excised, and the uptake of Cy5.5 labeled-[S]-nanomedicines by macrophages and monocytes was quantified. Interestingly, distinct uptake patterns for the three [S]-nanomedicines by aortic macrophages and Ly6C^{high} monocytes were found (Fig. 4C and D). The HDL formulation showed relatively high uptake by aortic macrophages, in line with what was previously reported in atherosclerosis and cancer models [44,47]. Interestingly, [S]-PM showed a similar degree of high uptake, not only by aortic macrophages but also by Ly6C^{high} monocytes. On the other hand, [S]-LIP demonstrated the lowest macrophage/monocyte targeting efficiency in comparison to the other two formulations (Fig. 4C and D).

Although our efficacy readout parameter for [S]-nanomedicine treatment was reduction in aortic plaque macrophage/monocyte content, uptake by other immune cell types present in the blood pool and spleen may affect treatment outcome. Similar to our findings in the aorta, [S]-PM showed a much higher affinity for blood Ly6C^{high} monocytes in comparison to [S]-HDL and [S]-LIP (~10 fold and ~5 fold, respectively, Supporting Fig. 7). Similarly, the association of [S]-PM with blood dendritic cells (DC) was also much higher than for [S]-HDL and [S]-LIP (~29 fold and 8 fold, respectively, Supporting Fig. 7). Also, in the spleen (Supporting Fig. 8), [S]-PM showed superior targeting efficiency towards the phagocytic target cells.

3.6. Therapeutic efficacy and safety

Reducing the number of plaque macrophages has been shown to decrease vessel wall inflammation and improve therapeutic outcomes in several key studies [8,10,39]. Also, blocking the recruitment of pro-inflammatory monocytes is a rational strategy to reduce inflammation in atherosclerotic plaques [68] and other diseases [69,70]. Here, we quantitatively assessed the efficacy of [S]-nanomedicine treatment by evaluating plaque macrophage/monocyte content using flow cytometry. *Apoe*$^{-/-}$ mice with advanced atherosclerosis were administered three doses of [S]-HDL, [S]-PM, [S]-LIP (60 mg/Kg simvastatin per dose), equivalent oral simvastatin (as control), or PBS i.v. (as placebo) (Fig. 5A). All mice (n = 8–10/group) were age-matched and received the assigned treatments within a single week. Aortic macrophages and pro-inflammatory Ly6C^{high} monocytes were gated as described before in Fig. 4B. As compared to the controls saline and oral simvastatin, a significant decrease in plaque macrophage content was observed in the [S]-PM and [S]-HDL treatment groups (Fig. 5B). [S]-LIP and oral [S] treatment groups did not yield significant reductions in plaque macrophage content (vs. saline treatment). Interestingly, none of the

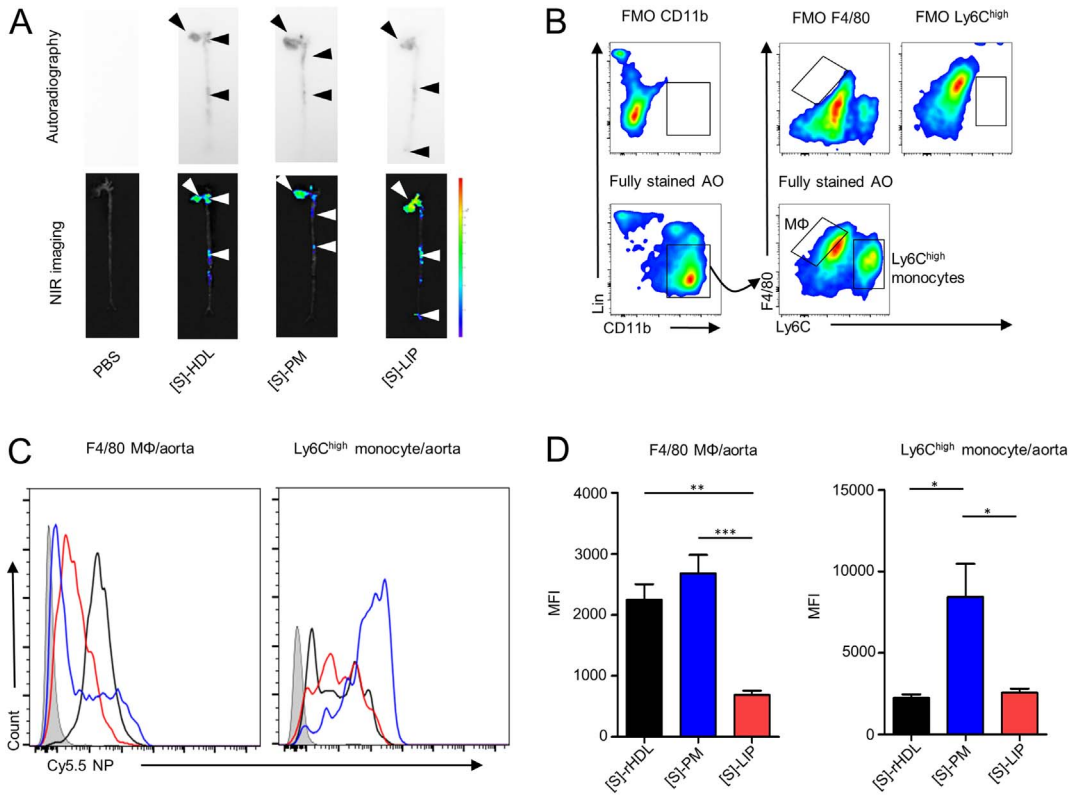

Fig. 4. Plaque targeting and uptake of [S]-nanomedicines by macrophages and monocytes in *Apoe*$^{-/-}$ mice with advanced atherosclerosis. (A) Autoradiography (upper panel) and NIRF (lower panel) images of excised aortas from *Apoe*$^{-/-}$ mice 24 h after injection. (B) Flow cytometry gating procedures and fluorescence minus one (FMO) control samples to identify aortic macrophages (MΦ) and Ly6C^{high} monocytes. (C) Black ([S]-HDL), blue ([S]-PM), and red ([S]-LIP) histograms showing representative signal distribution of aortic macrophages and Ly6C^{high} monocytes in mice injected with the [S]-nanomedicines compared with the cells from control animals injected with PBS (gray histogram on the left in each graph). (D) Quantification of mean fluorescence intensity (MFI) of macrophages and monocytes in the atherosclerotic aortas (n = 4 per condition). [S]: simvastatin; HDL: high density lipoprotein; PM: polymeric micelles; LIP: liposomes; NIR: near-infrared; FMO: fluorescence minus one; MΦ: macrophages; lin: lineage; Cy5.5 NP: cyanine 5.5 labeled nanoparticles. Data presented as mean ± SEM. *$P \leq 0.05$; **$P \leq 0.01$; ***$P \leq 0.001$. (For interpretation of the references to colour in this figure legend, the reader is referred to the web version of this article.)

nanomedicine treatments had a statistically significant impact on plaque Ly6C^{high} monocyte content, indicating that the different treatments did not affect monocyte recruitment, in line with what we observed previously [38,39].

We further analyzed blood as the direct recruitment pool for monocytes and other immune cells. None of the treatment groups showed a significant change in the number of total circulating leukocytes, monocytes, neutrophils, lymphocytes, red blood cells (RBCs), or platelets (vs. saline) (Fig. 5C). Additionally, the [S]-nanomedicine treatments did not significantly alter the concentration of serum triglycerides, total cholesterol, and glucose (vs. oral [S] treatment or placebo) (Supporting Fig. 9). Similarly, no significant concentration changes were found in toxicity blood markers (Supporting Fig. 9).

Nanomedicines are developed to ultimately achieve local, targeted drug delivery to pathological lesions (atherosclerotic plaques in our study) upon intravenous injection, aiming to improve the therapeutic efficacy and safety profile of the free drug. Nanocarrier characteristics such as composition, size, and morphology, which likely affect their circulation kinetics, drug release kinetics, extravasation, penetration, and importantly, specificity to the target cell(s), will have a direct impact on the therapeutic efficacy of nanomedicines. In our study, all treatments contained the same drug, the HMG-CoA reductase inhibitor simvastatin, which was administered at the same dose, and evaluated in age/diet matched *Apoe*$^{-/-}$ mice, a well-established model of atherosclerosis [71].

In our head-to-head study, we found the [S]-LIP yielded the least efficacy in reducing macrophage burden in atherosclerotic plaques. Although [S]-LIP possessed a long blood half-life, its poor plaque macrophage targeting efficiency, in addition to leakage of simvastatin from liposomes in circulation, might have contributed to this low efficacy. On the contrary, despite its comparatively shorter circulation half-life, [S]-HDL demonstrated better efficacy than [S]-LIP. This noticeable difference is probably due to HDL's high specificity for plaque macrophages. These results also suggest that HDL can be an ideal imaging probe for lesion-associated macrophages [44,50]. Among the three platforms, [S]-PM demonstrated the most favorable features of a targeted drug delivery approach, including long circulation times, increased drug-nanocarrier stability in serum, and improved cellular targeting efficiency. These features resulted in the most prominent reduction in plaque macrophage burden. Remarkably, although the three nanomedicines showed uptake by pro-inflammatory Ly6C^{high} monocytes, especially [S]-PM, none of the treatments altered monocyte content in atherosclerotic plaques. These different treatment effects on plaque macrophages and monocytes are in line with the new paradigm that considers atherosclerosis as a multiphasic process in which local macrophage proliferation, rather than monocyte recruitment, governs advanced atherosclerotic plaque progression [8,72]. Thus, tackling monocyte recruitment in advanced atherosclerosis with (nano-) medicines may not be an ideal approach for atheroprotection as demonstrated by Lindau et al. [73]. However, blocking the recruitment of pro-inflammatory monocytes may be imperative in conditions/diseases in which active monocytosis and recruitment can exacerbate the inflammatory response. An example of these conditions is the rapid monocyte kinetics triggered by acute myocardial infarction [68].

Additionally, the three [S]-nanomedicines did not change the metabolic parameters in plasma nor significantly alter major biomarkers of HMG-CoA reductase inhibitor-induced myo- or hepatotoxicity [37]. Moreover, HDL - one of our body's own nanoparticles - and liposomes are well known for their biocompatibility and biodegradability. PM composed of pHPMA polymers are also known to be non-immunogenic

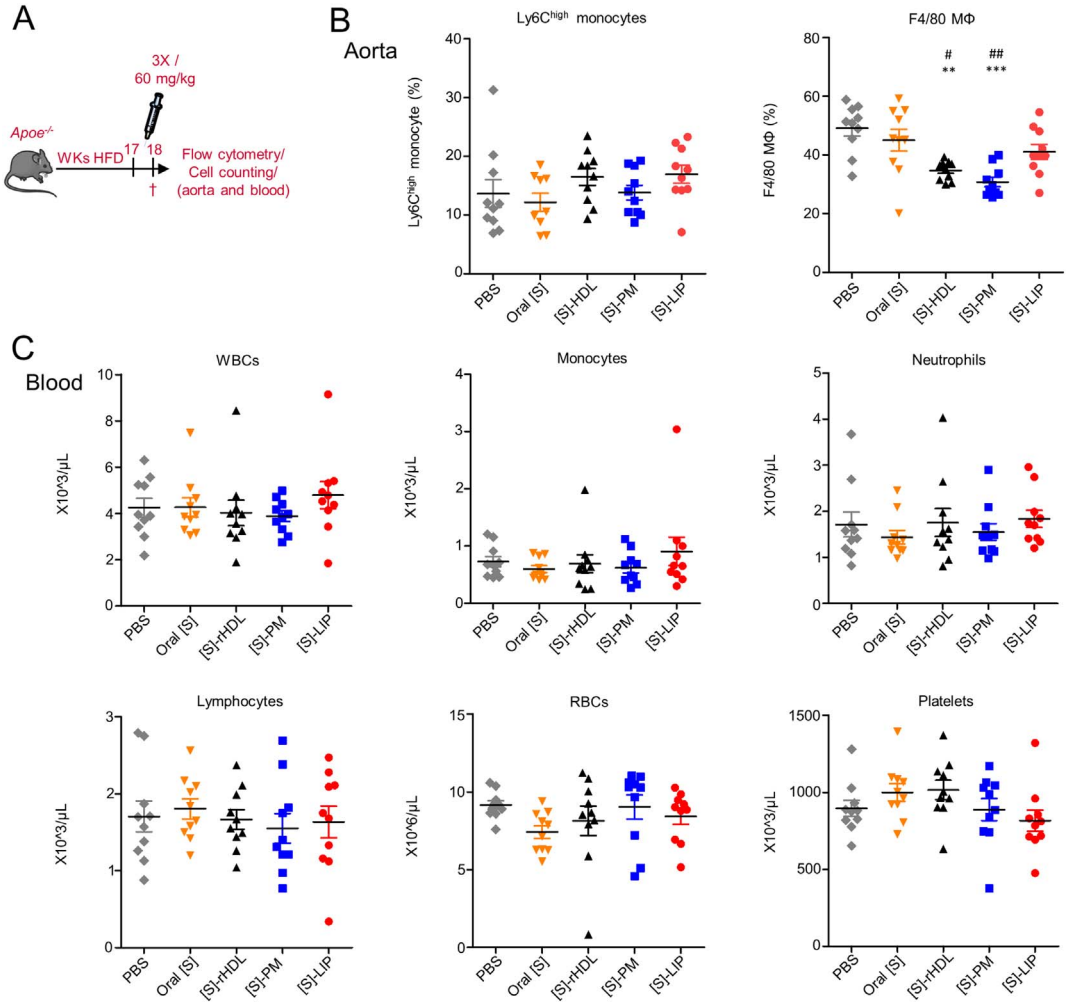

Fig. 5. Therapeutic efficacy of [S]-nanomedicines. (A) A schematic depiction of the efficacy study, in which *Apoe*$^{-/-}$ mice were administered 60 mg/kg simvastatin i.v., for [S]-nanomedicines, oral gavage (control group), or PBS (placebo) for one week. (B) Quantification of aortic Ly6C^{high} monocytes and macrophages using flow cytometry (percentage of CD45^{+} total aortic leukocytes). (C) Complete blood count analysis. (n = 8–10 per condition). *Apoe*$^{-/-}$: apolipoprotein *E*-deficient; PBS: phosphate buffered saline; [S]: simvastatin; HDL: high density lipoprotein; PM: polymeric micelles; LIP: liposomes; Wks: weeks; HFD: high fat diet; MΦ: macrophages; WBCs; white blood cells, RBCs; red blood cells. Data presented as mean ± SEM. *$P \leq 0.05$; **$P \leq 0.01$; ***$P \leq 0.001$. *relative to the PBS group. #relative to oral [S].

and biocompatible [74–76]; they have been extensively investigated for drug delivery (reviewed by Talelli et al. [56]) Moreover, several pHPMA-based therapies have been clinically evaluated (reviewed by Duncan and Vicent [77]). Our data indicate the safety of our treatments, an important step for the potential clinical translation of the nanomedicines under investigation. However, more detailed safety studies will need to be executed before any clinical application. Furthermore, factors such manufacturability under good manufacture practice (GMP) conditions, cost, patient selection, and best therapeutic approach (e.g. high dose short-term injections with and without oral therapy) also need to be carefully considered for clinical translation [78].

4. Conclusions

In this systematic head-to-head study, we have adopted sensitive, quantitative techniques to evaluate three clinically applicable nanomedicines targeting HMG-CoA reductase, in regards to their physicochemical characteristics and *in vivo* performance in *Apoe*$^{-/-}$ mice with advanced atherosclerosis. It was found that [S]-PM possesses superior efficacy, in comparison to [S]-HDL and [S]-LIP, to locally reduce the macrophage burden in advanced atherosclerotic plaques. This is likely due to the higher targeted drug delivery efficiency, as a result of the combination of the enhanced retention of simvastatin in the polymeric micelles and the high cellular targeting efficiency to plaque macrophages. These findings are crucial for further development and clinical application of nanomedicines to reduce inflammation in advanced atherosclerosis. Furthermore, the work presented in this paper suggests that the systematic investigation of nanomaterials, beyond cancer, is crucial for the future of nanomedicine design, optimization, and clinical applicability in several disease contexts.

Acknowledgements

We thank Dr. Robbert Jan Kok and Jeffrey Ritsema (Utrecht University) for the valuable discussion. We would also like to thank The Small Animal Imaging Core, The Radiochemistry and Molecular Imaging Probes Core at Memorial Sloan Kettering Cancer Center as well as the Flow Cytometry Core Facility and The Preclinical Imaging Center of Translational and Molecular Imaging Institute of Icahn School of Medicine at Mount Sinai for their support. This work was supported by a European Framework Program 7 grant (FP7-Health 309820: NanoAthero to G.S. and A.A.), by National Institute of Health Grants R01 HL118440, R01HL125703, a Netherlands Organisation for Scientific Research Vidi (all to W.J.M.M.), R01 EB009638 (to Z.A.F.), as well as P30 CA008748 (to T.R.) and Foundation “De Drie Lichten” in The Netherlands (M.L.S.).

Appendix A. Supplementary data

Supplementary data to this article can be found online at http://dx.doi.org/10.1016/j.jconrel.2017.07.013.

References

[1] E. Falk, Pathogenesis of atherosclerosis, J. Am. Coll. Cardiol. 47 (2006) C7–C12, http://dx.doi.org/10.1016/j.jacc.2005.09.068.

[2] P. Libby, History of discovery : inflammation in atherosclerosis, Arter. Thromb. Vasc. Biol. 32 (2012) 2045–2051, http://dx.doi.org/10.1161/ATVBAHA.108.179705.

[3] G.K. Hansson, A. Hermansson, The immune system in atherosclerosis, Nat. Immunol. 12 (2011) 204–212, http://dx.doi.org/10.1038/ni.2001.

[4] K.J. Moore, F.J. Sheedy, E.A. Fisher, Macrophages in atherosclerosis: a dynamic balance, Nat. Rev. 13 (2013) 709–721, http://dx.doi.org/10.1038/nri3520.

[5] S. Blankenberg, S. Barbaux, L. Tiret, Adhesion molecules and atherosclerosis, Atherosclerosis 170 (2003) 191–203 (doi: S0021-9150(03)00097-2 [pii]).

[6] K.J. Woollard, F. Geissmann, Monocytes in atherosclerosis: subsets and functions, Nat. Rev. Cardiol. 7 (2010) 77–86, http://dx.doi.org/10.1038/nrcardio.2009.228.

[7] J.F. Bentzon, F. Otsuka, R. Virmani, E. Falk, Mechanisms of plaque formation and rupture, Circ. Res. 114 (2014).

[8] C.S. Robbins, I. Hilgendorf, G.F. Weber, I. Theurl, Y. Iwamoto, J.-L.L. Figueiredo, R. Gorbatov, G.K. Sukhova, L.M.S. Gerhardt, D. Smyth, C.C.J. Zavitz, E.A. Shikatani, M. Parsons, N. van Rooijen, H.Y. Lin, M. Husain, P. Libby, M. Nahrendorf, R. Weissleder, F.K. Swirski, Local proliferation dominates lesional macrophage accumulation in atherosclerosis, Nat. Med. 19 (2013) 1166–1172, http://dx.doi.org/10.1038/nm.3258.

[9] K.J. Moore, I. Tabas, Macrophages in the pathogenesis of atherosclerosis, Cell 145 (2011) 341–355, http://dx.doi.org/10.1016/j.cell.2011.04.005.

[10] P. Dutta, G. Courties, Y. Wei, F. Leuschner, R. Gorbatov, C.S. Robbins, Y. Iwamoto, B. Thompson, A.L. Carlson, T. Heidt, M.D. Majmudar, F. Lasitschka, M. Etzrodt, P. Waterman, M.T. Waring, A.T. Chicoine, A.M. van der Laan, H.W.M. Niessen, J.J. Piek, B.B. Rubin, J. Butany, J.R. Stone, H.A. Katus, S.A. Murphy, D.A. Morrow, M.S. Sabatine, C. Vinegoni, M.A. Moskowitz, M.J. Pittet, P. Libby, C.P. Lin, F.K. Swirski, R. Weissleder, M. Nahrendorf, Myocardial infarction accelerates atherosclerosis, Nature 487 (2012) 325–329, http://dx.doi.org/10.1038/nature11260.

[11] H. Emami, P. Singh, M. MacNabb, E. Vucic, Z. Lavender, J.H. Rudd, Z.A. Fayad, J. Lehrer-Graiwer, M. Korsgren, A.L. Figueroa, J. Fredrickson, B. Rubin, U. Hoffmann, Q.A. Truong, J.K. Min, A. Baruch, K. Nasir, M. Nahrendorf, A. Tawakol, Splenic metabolic activity predicts risk of future cardiovascular events: demonstration of a cardiosplenic axis in humans, JACC.Cardiovasc. Imaging 8 (2015) 121–130, http://dx.doi.org/10.1016/j.jcmg.2014.10.009.

[12] G.W. Stone, A. Maehara, A.J. Lansky, B. de Bruyne, E. Cristea, G.S. Mintz, R. Mehran, J. McPherson, N. Farhat, S.P. Marso, H. Parise, B. Templin, R. White, Z. Zhang, P.W. Serruys, A prospective natural-history study of coronary atherosclerosis, N. Engl. J. Med. 364 (2011) 226–235, http://dx.doi.org/10.1056/NEJMoa1002358.

[13] T. Lammers, F. Kiessling, W.E. Hennink, G. Storm, Drug targeting to tumors: principles, pitfalls and (pre-) clinical progress, J. Control. Release 161 (2012) 175–187, http://dx.doi.org/10.1016/j.jconrel.2011.09.063.

[14] Y.H. Bae, K. Park, Targeted drug delivery to tumors: myths, reality and possibility, J. Control. Release 153 (2011) 198–205, http://dx.doi.org/10.1016/j.jconrel.2011.06.001.

[15] D. Peer, J.M. Karp, S. Hong, O.C. Farokhzad, R. Margalit, R. Langer, Nanocarriers as an emerging platform for cancer therapy, Nat. Nanotechnol. 2 (2007) 751–760, http://dx.doi.org/10.1038/nnano.2007.387.

[16] V.P. Torchilin, Targeted pharmaceutical nanocarriers for cancer therapy and imaging, AAPS J. 9 (2007) E128–E147, http://dx.doi.org/10.1208/aapsj0902015.

[17] K.F. Timbie, U. Afzal, A. Date, C. Zhang, J. Song, G. Wilson Miller, J.S. Suk, J. Hanes, R.J. Price, MR image-guided delivery of cisplatin-loaded brain-penetrating nanoparticles to invasive glioma with focused ultrasound, J. Control. Release (2017), http://dx.doi.org/10.1016/j.jconrel.2017.03.017.

[18] B.J. Crielaard, T. Lammers, R.M. Schiffelers, G. Storm, Drug targeting systems for inflammatory disease: one for all, all for one, J. Control. Release 161 (2012) 225–234, http://dx.doi.org/10.1016/j.jconrel.2011.12.014.

[19] B. Ozbakir, B.J. Crielaard, J.M. Metselaar, G. Storm, T. Lammers, Liposomal corticosteroids for the treatment of inflammatory disorders and cancer, J. Control. Release 190 (2014) 624–636, http://dx.doi.org/10.1016/j.jconrel.2014.05.039.

[20] T.M. Allen, P.R. Cullis, Liposomal drug delivery systems: from concept to clinical applications, Adv. Drug Deliv. Rev. 65 (2013) 36–48, http://dx.doi.org/10.1016/j.addr.2012.09.037.

[21] R. Weissleder, M. Nahrendorf, M.J. Pittet, Imaging macrophages with nanoparticles, Nat. Mater. 13 (2014) 125–138, http://dx.doi.org/10.1038/nmat3780.

[22] J.A. Hubbell, A. Chilkoti, Nanomaterials for drug delivery, Science 80 (2012) 337.

[23] C. Oerlemans, W. Bult, M. Bos, G. Storm, J.F.W. Nijsen, W.E. Hennink, Polymeric micelles in anticancer therapy: targeting, imaging and triggered release, Pharm. Res. 27 (2010) 2569–2589, http://dx.doi.org/10.1007/s11095-010-0233-4.

[24] C. Deng, Y. Jiang, R. Cheng, F. Meng, Z. Zhong, Biodegradable polymeric micelles for targeted and controlled anticancer drug delivery: promises, progress and prospects, Nano Today 7 (2012) 467–480, http://dx.doi.org/10.1016/j.nantod.2012.08.005.

[25] K.K. Ng, J.F. Lovell, G. Zheng, Lipoprotein-inspired nanoparticles for cancer theranostics, Acc. Chem. Res. 44 (2011) 1105–1113, http://dx.doi.org/10.1021/ar200017e.

[26] B.A. Kingwell, M.J. Chapman, A. Kontush, N.E. Miller, HDL-targeted therapies: progress, failures and future, Nat. Rev. Drug Discov. 13 (2014) 445–464, http://dx.doi.org/10.1038/nrd4279.

[27] H. Cabral, K. Kataoka, Progress of drug-loaded polymeric micelles into clinical studies, J. Control. Release 190 (2014) 465–476, http://dx.doi.org/10.1016/j.jconrel.2014.06.042.

[28] S. Mitragotri, T. Lammers, Y.H. Bae, S. Schwendeman, S. De Smedt, J.-C. Leroux, D. Peer, I.C. Kwon, H. Harashima, A. Kikuchi, Y.-K. Oh, V. Torchilin, W. Hennink, J. Hanes, K. Park, Drug delivery research for the future: expanding the nano horizons and beyond, J. Control. Release 246 (2017) 183–184, http://dx.doi.org/10.1016/j.jconrel.2017.01.011.

[29] T. Lammers, F. Kiessling, M. Ashford, W. Hennink, D. Crommelin, G. Strom, Cancer nanomedicine: is targeting our target? Nat. Rev. Mater. 1 (2016) 16069, , http://dx.doi.org/10.1038/natrevmats.2016.69.

[30] Y. Min, J.M. Caster, M.J. Eblan, A.Z. Wang, Clinical translation of nanomedicine, Chem. Rev. 115 (2015) 11147–11190, http://dx.doi.org/10.1021/acs.chemrev.5b00116.

[31] J.L. Goldstein, M.S. Brown, Regulation of the mevalonate pathway, Nature 343 (1990) 425–430, http://dx.doi.org/10.1038/343425a0.

[32] J.K. Liao, U. Laufs, Pleiotropic effects of statins, Annu. Rev. Pharmacol. Toxicol. 45 (2005) 89–118, http://dx.doi.org/10.1146/annurev.pharmtox.45.120403.095748.

[33] A. Alaarg, K.H. Zheng, F.M. van der Valk, A.E. da Silva, M. Versloot, L.C. van Ufford, D.M. Schulte, G. Storm, J.M. Metselaar, E.S.G. Stroes, A.A. Hamers, Multiple pathway assessment to predict anti-atherogenic efficacy of drugs targeting macrophages in atherosclerotic plaques, Vascul. Pharmacol. 82 (2015), http://dx.doi.org/10.1016/j.vph.2016.04.006.

[34] A. Tawakol, Z.A. Fayad, R. Mogg, A. Alon, M.T. Klimas, H. Dansky, S.S. Subramanian, A. Abdelbaky, J.H.F. Rudd, M.E. Farkouh, I.O. Nunes, C.R. Beals, S.S. Shankar, Intensification of statin therapy results in a rapid reduction in atherosclerotic inflammation: results of a multicenter fluorodeoxyglucose-positron emission tomography/computed tomography feasibility study, J. Am. Coll. Cardiol. 62 (2013) 909–917, http://dx.doi.org/10.1016/j.jacc.2013.04.066.

[35] C.P. Sparrow, C.A. Burton, M. Hernandez, S. Mundt, H. Hassing, S. Patel, R. Rosa, A. Hermanowski-Vosatka, P.-R. Wang, D. Zhang, L. Peterson, P.A. Detmers, Y.-S. Chao, S.D. Wright, Simvastatin has anti-inflammatory and antiatherosclerotic activities independent of plasma cholesterol lowering, Arterioscler. Thromb. Vasc. Biol. 21 (2001).

[36] J. Armitage, The safety of statins in clinical practice, Lancet 370 (2007) 1781–1790, http://dx.doi.org/10.1016/S0140-6736(07)60716-8.

[37] S. Bellosta, R. Paoletti, A. Corsini, Safety of statins: focus on clinical pharmacokinetics and drug interactions, Circulation 109 (2004), http://dx.doi.org/10.1161/01.CIR.0000131519.15067.1f (III-50-III-57).

[38] R. Duivenvoorden, J. Tang, D.P. Cormode, A.J. Mieszawska, D. Izquierdo-Garcia, C. Ozcan, M.J. Otten, N. Zaidi, M.E. Lobatto, S.M. van Rijs, B. Priem, E.L. Kuan, C. Martel, B. Hewing, H. Sager, M. Nahrendorf, G.J. Randolph, E.S.G. Stroes, V. Fuster, E.A. Fisher, Z.A. Fayad, W.J.M. Mulder, A statin-loaded reconstituted high-density lipoprotein nanoparticle inhibits atherosclerotic plaque inflammation, Nat. Commun. 5 (2014) 227–239, http://dx.doi.org/10.1038/ncomms4065.

[39] J. Tang, M.E. Lobatto, L. Hassing, S. van der Staay, S.M. van Rijs, C. Calcagno, M.S. Braza, S. Baxter, F. Fay, B.L. Sanchez-Gaytan, R. Duivenvoorden, H.B. Sager, Y.M. Astudillo, W. Leong, S. Ramachandran, G. Storm, C. Perez-Medina, T. Reiner, D.P. Cormode, G.J. Strijkers, E.S.G. Stroes, F.K. Swirski, M. Nahrendorf, E.A. Fisher, Z.A. Fayad, W.J.M. Mulder, Inhibiting macrophage proliferation suppresses atherosclerotic plaque inflammation, Sci. Adv. 1 (2015) e1400223(doi:e1400223 [pii]).

[40] Y. Shi, R. Van Der Meel, B. Theek, E. Oude Blenke, E.H.E. Pieters, M.H.A.M. Fens, J. Ehling, R.M. Schiffelers, G. Storm, C.F. Van Nostrum, T. Lammers, W.E. Hennink, Complete regression of xenograft tumors upon targeted delivery of paclitaxel via π-π stacking stabilized polymeric micelles, ACS Nano 9 (2015) 3740–3752, http://dx.doi.org/10.1021/acsnano.5b00929.

[41] C. Pérez-Medina, D. Abdel-Atti, Y. Zhang, V.A. Longo, C.P. Irwin, T. Binderup, J. Ruiz-Cabello, Z.A. Fayad, J.S. Lewis, W.J.M. Mulder, T. Reiner, A modular labeling strategy for in vivo PET and near-infrared fluorescence imaging of nanoparticle tumor targeting, J. Nucl. Med. 55 (2014) 1706–1712, http://dx.doi.org/10.2967/jnumed.114.141861.

[42] M. Banciu, J.M. Metselaar, R.M. Schiffelers, G. Storm, Antitumor activity of liposomal prednisolone phosphate depends on the presence of functional tumor-associated macrophages in tumor tissue, Neoplasia 10 (2008) 108–117, http://dx.doi.org/10.1593/neo.07913.

[43] M.E. Lobatto, C. Calcagno, A. Millon, M.L. Senders, F. Fay, P.M. Robson, S. Ramachandran, T. Binderup, M.P. Paridaans, S. Sensarn, S. Rogalla, R.E. Gordon, L. Cardoso, G. Storm, J.M. Metselaar, C.H. Contag, E.S. Stroes, Z.A. Fayad, W.J. Mulder, Atherosclerotic plaque targeting mechanism of long-circulating nanoparticles established by multimodal imaging, ACS Nano 9 (2015) 1837–1847, http://dx.doi.org/10.1021/nn506750r.

[44] C. Pérez-Medina, J. Tang, D. Abdel-Atti, B. Hogstad, M. Merad, E.A. Fisher, Z.A. Fayad, J.S. Lewis, W.J.M. Mulder, T. Reiner, C. Perez-Medina, J. Tang, D. Abdel-Atti, B. Hogstad, M. Merad, E.A. Fisher, Z.A. Fayad, J.S. Lewis, W.J.M. Mulder, T. Reiner, P.E.T. Imaging, Of tumor-associated macrophages with 89Zr-labeled high-density lipoprotein nanoparticles, J. Nucl. Med. 56 (2015) 1272–1277, http://dx.doi.org/10.2967/jnumed.115.158956.

[45] Y. Zhao, F. Fay, S. Hak, J. Manuel Perez-Aguilar, B.L. Sanchez-Gaytan, B. Goode, R. Duivenvoorden, C. de Lange Davies, A. Bjorkoy, H. Weinstein, Z.A. Fayad, C. Perez-Medina, W.J.M. Mulder, A. Bjørkøy, H. Weinstein, Z.A. Fayad, C. Pérez-Medina, W.J.M. Mulder, Augmenting drug-carrier compatibility improves tumour

nanotherapy efficacy, Nat. Commun. 7 (2016) 11221, http://dx.doi.org/10.1038/ncomms11221.
[46] J.Z. Nordin, Y. Lee, P. Vader, I. Mäger, H.J. Johansson, W. Heusermann, O.P.B. Wiklander, M. Hällbrink, Y. Seow, J.J. Bultema, J. Gilthorpe, T. Davies, P.J. Fairchild, S. Gabrielsson, N.C. Meisner-Kober, J. Lehtiö, C.I.E. Smith, M.J.A. Wood, S. EL Andaloussi, Ultrafiltration with size-exclusion liquid chromatography for high yield isolation of extracellular vesicles preserving intact biophysical and functional properties, Nanomed. Nanotechnol. Biol. Med. 11 (2015) 879–883, http://dx.doi.org/10.1016/j.nano.2015.01.003.
[47] J. Tang, S. Baxter, A. Menon, A. Alaarg, B.L. Sanchez-Gaytan, F. Fay, Y. Zhao, M. Ouimet, M.S. Braza, V.A. Longo, D. Abdel-Atti, R. Duivenvoorden, C. Calcagno, G. Storm, S. Tsimikas, K.J. Moore, F.K. Swirski, M. Nahrendorf, E.A. Fisher, C. Pérez-Medina, Z.A. Fayad, T. Reiner, W.J.M. Mulder, Immune cell screening of a nanoparticle library improves atherosclerosis therapy, Proc. Natl. Acad. Sci. U. S. A. 113 (2016), http://dx.doi.org/10.1073/pnas.1609629113.
[48] M.E. Lobatto, Z.A. Fayad, S. Silvera, E. Vucic, C. Calcagno, V. Mani, S.D. Dickson, K. Nicolay, M. Banciu, R.M. Schiffelers, J.M. Metselaar, L. van Bloois, H.S. Wu, J.T. Fallon, J.H. Rudd, V. Fuster, E.A. Fisher, G. Storm, W.J. Mulder, Multimodal clinical imaging to longitudinally assess a nanomedical anti-inflammatory treatment in experimental atherosclerosis, Mol. Pharm. 7 (2010) 2020–2029, http://dx.doi.org/10.1021/mp100309y.
[49] F.M. van der Valk, D.F. van Wijk, M.E. Lobatto, H.J. Verberne, G. Storm, M.C.M. Willems, D.A. Legemate, A.J. Nederveen, C. Calcagno, V. Mani, S. Ramachandran, M.P.M. Paridaans, M.J. Otten, G.M. Dallinga-Thie, Z.A. Fayad, M. Nieuwdorp, D.M. Schulte, J.M. Metselaar, W.J.M. Mulder, E.S. Stroes, Prednisolone-containing liposomes accumulate in human atherosclerotic macrophages upon intravenous administration, Nanomedicine 11 (2015) 1039–1046, http://dx.doi.org/10.1016/j.nano.2015.02.021.
[50] C. Pérez-Medina, T. Binderup, M.E. Lobatto, J. Tang, C. Calcagno, L. Giesen, C.H. Wessel, J. Witjes, S. Ishino, S. Baxter, Y. Zhao, S. Ramachandran, M. Eldib, B.L. Sánchez-Gaytán, P.M. Robson, J. Bini, J.F. Granada, K.M. Fish, E.S.G. Stroes, R. Duivenvoorden, S. Tsimikas, J.S. Lewis, T. Reiner, V. Fuster, A. Kjær, E.A. Fisher, Z.A. Fayad, W.J.M. Mulder, In vivo PET imaging of hdl in multiple atherosclerosis models, JACC Cardiovasc. Imaging 9 (2016) 950–961, http://dx.doi.org/10.1016/j.jcmg.2016.01.020.
[51] B.L. Sanchez-Gaytan, F. Fay, M.E. Lobatto, J. Tang, M. Ouimet, Y. Kim, S.E.M. van der Staay, S.M. van Rijs, B. Priem, L. Zhang, E.A. Fisher, K.J. Moore, R. Langer, Z.A. Fayad, W.J.M. Mulder, HDL-mimetic PLGA nanoparticle to target atherosclerosis plaque macrophages, Bioconjug. Chem. 26 (2015) 443–451, http://dx.doi.org/10.1021/bc500517k.
[52] O. Naksuriya, Y. Shi, C.F. Van Nostrum, S. Anuchapreeda, W.E. Hennink, S. Okonogi, HPMA-based polymeric micelles for curcumin solubilization and inhibition of cancer cell growth, Eur. J. Pharm. Biopharm. 94 (2015) 501–512, http://dx.doi.org/10.1016/j.ejpb.2015.06.010.
[53] Y. Shi, T. Lammers, G. Storm, W.E. Hennink, Physico-chemical strategies to enhance stability and drug retention of polymeric micelles for tumor-targeted drug delivery, Macromol. Biosci. 17 (2017) 1600160, , http://dx.doi.org/10.1002/mabi.201600160.
[54] Y. Zhang, T. Ren, J. Gou, L. Zhang, X. Tao, B. Tian, P. Tian, D. Yu, J. Song, X. Liu, Y. Chao, W. Xiao, X. Tang, Strategies for improving the payload of small molecular drugs in polymeric micelles, J. Control. Release (2017), http://dx.doi.org/10.1016/j.jconrel.2017.01.047.
[55] L. Quan, Y. Zhang, B.J. Crielaard, A. Dusad, S.M. Lele, C.J. Rijcken, J.M. Metselaar, H. Kostkova, T. Etrych, K. Ulbrich, F. Kiessling, T.R. Mikuls, W.E. Hennink, G. Storm, T. Lammers, D. Wang, Nanomedicines for inflammatory arthritis: head-to-head comparison of glucocorticoid-containing polymers, micelles, and liposomes, ACS Nano 8 (2014) 458–466, http://dx.doi.org/10.1021/nn4048205.
[56] M. Talelli, C.J.F. Rijcken, C.F. van Nostrum, G. Storm, W.E. Hennink, Micelles based on HPMA copolymers? Adv. Drug Deliv. Rev. 62 (2010) 231–239, http://dx.doi.org/10.1016/j.addr.2009.11.029.
[57] A.G. Lacko, N.A. Sabnis, B. Nagarajan, W.J. McConathy, HDL as a drug and nucleic acid delivery vehicle, Front. Pharmacol. 6 (2015) 247, http://dx.doi.org/10.3389/fphar.2015.00247.
[58] B.L. Sanchez-Gaytan, F. Fay, S. Hak, A. Alaarg, Z.A. Fayad, C. Pérez-Medina, W.J.M. Mulder, Y. Zhao, Real-time monitoring of nanoparticle formation by FRET imaging, Angew. Chem. Int. Ed. (2017), http://dx.doi.org/10.1002/anie.201611288.
[59] Y. Shi, S. Kunjachan, Z. Wu, F. Gremse, D. Moeckel, M. van Zandvoort, F. Kiessling, G. Storm, C.F. van Nostrum, W.E. Hennink, T. Lammers, Fluorophore labeling of core-crosslinked polymeric micelles for multimodal *in vivo* and *ex vivo* optical imaging, Nanomedicine 10 (2015) 1111–1125, http://dx.doi.org/10.2217/nnm.14.170.
[60] B.M. Zeglis, P. Mohindra, G.I. Weissmann, V. Divilov, S.A. Hilderbrand, R. Weissleder, J.S. Lewis, Modular strategy for the construction of Radiometalated antibodies for positron emission tomography based on inverse electron demand Diels–Alder click chemistry, Bioconjug. Chem. 22 (2011) 2048–2059, http://dx.doi.org/10.1021/bc200288d.
[61] S. Kunjachan, J. Ehling, G. Storm, F. Kiessling, T. Lammers, Noninvasive imaging of nanomedicines and nanotheranostics: principles, progress, and prospects, Chem. Rev. 115 (2015) 10907–10937, http://dx.doi.org/10.1021/cr500314d.
[62] T. Lammers, SMART drug delivery systems: back to the future vs. clinical reality, Int. J. Pharm. 454 (2013) 527–529, http://dx.doi.org/10.1016/j.ijpharm.2013.02.046.
[63] H.S. Choi, W. Liu, P. Misra, E. Tanaka, J.P. Zimmer, B. Itty Ipe, M.G. Bawendi, J.V. Frangioni, Renal clearance of quantum dots, Nat. Biotechnol. 25 (2007) 1165–1170, http://dx.doi.org/10.1038/nbt1340.
[64] E.J. Keliher, Y.-X. Ye, G.R. Wojtkiewicz, A.D. Aguirre, B. Tricot, M.L. Senders, H. Groenen, F. Fay, C. Perez-Medina, C. Calcagno, G. Carlucci, T. Reiner, Y. Sun, G. Courties, Y. Iwamoto, H.-Y. Kim, C. Wang, J.W. Chen, F.K. Swirski, H.-Y. Wey, J. Hooker, Z.A. Fayad, W.J.M. Mulder, R. Weissleder, M. Nahrendorf, Polyglucose nanoparticles with renal elimination and macrophage avidity facilitate PET imaging in ischaemic heart disease, Nat. Commun. 8 (2017) 14064, , http://dx.doi.org/10.1038/ncomms14064.
[65] V.V. Itskovich, R.P. Choudhury, J.G.S. Aguinaldo, J.T. Fallon, S. Omerhodzic, E.A. Fisher, Z.A. Fayad, Characterization of aortic root atherosclerosis in ApoE knockout mice: high-resolution in vivo and ex vivo MRM with histological correlation, Magn. Reson. Med. 49 (2003) 381–385, http://dx.doi.org/10.1002/mrm.10360.
[66] J. Baglione, J.D. Smith, Quantitative assay for mouse atherosclerosis in the aortic root, Cardiovasc. Dis. Vol. 2 Mol. Med, Humana Press, New Jersey, 2006, pp. 83–96, , http://dx.doi.org/10.1385/1-59745-213-0:83.
[67] G.S. Getz, C.A. Reardon, Animal models of atherosclerosis, Arterioscler. Thromb. Vasc. Biol. 32 (2012) 1104–1115, http://dx.doi.org/10.1161/ATVBAHA.111.237693.
[68] F. Leuschner, P. Dutta, R. Gorbatov, T.I. Novobrantseva, J.S. Donahoe, G. Courties, K.M. Lee, J.I. Kim, J.F. Markmann, B. Marinelli, P. Panizzi, W.W. Lee, Y. Iwamoto, S. Milstein, H. Epstein-Barash, W. Cantley, J. Wong, V. Cortez-Retamozo, A. Newton, K. Love, P. Libby, M.J. Pittet, F.K. Swirski, V. Koteliansky, R. Langer, R. Weissleder, D.G. Anderson, M. Nahrendorf, Therapeutic siRNA silencing in inflammatory monocytes in mice, Nat. Biotechnol. 29 (2011) 1005–1010, http://dx.doi.org/10.1038/nbt.1989.
[69] E. Zigmond, C. Varol, J. Farache, E. Elmaliah, A.T. Satpathy, G. Friedlander, M. Mack, N. Shpigel, I.G. Boneca, K.M. Murphy, G. Shakhar, Z. Halpern, S. Jung, Ly6Chi monocytes in the inflamed colon give rise to proinflammatory effector cells and migratory antigen-presenting cells, Immunity 37 (2012) 1076–1090, http://dx.doi.org/10.1016/j.immuni.2012.08.026.
[70] H.-J. Anders, V. Ninichuk, D. Schlöndorff, Progression of kidney disease: blocking leukocyte recruitment with chemokine receptor CCR1 antagonists, Kidney Int. 69 (2006) 29–32, http://dx.doi.org/10.1038/sj.ki.5000053.
[71] K.S. Meir, E. Leitersdorf, Atherosclerosis in the apolipoprotein E–deficient mouse, Arterioscler. Thromb. Vasc. Biol. 24 (2004).
[72] F.K. Swirski, I. Hilgendorf, C.S. Robbins, From proliferation to proliferation: monocyte lineage comes full circle, Semin. Immunopathol. 36 (2014) 137–148, http://dx.doi.org/10.1007/s00281-013-0409-1.
[73] A. Lindau, C. Härdtner, S.P. Hergeth, K.D. Blanz, B. Dufner, N. Hoppe, N. Anto-Michel, J. Kornemann, J. Zou, L.M.S. Gerhardt, T. Heidt, F. Willecke, S. Geis, P. Stachon, D. Wolf, P. Libby, F.K. Swirski, C.S. Robbins, W. McPheat, S. Hawley, M. Braddock, R. Gilsbach, L. Hein, C. von zur Mühlen, C. Bode, A. Zirlik, I. Hilgendorf, C. Hardtner, S.P. Hergeth, K.D. Blanz, B. Dufner, N. Hoppe, N. Anto-Michel, J. Kornemann, J. Zou, L.M.S. Gerhardt, T. Heidt, F. Willecke, S. Geis, P. Stachon, D. Wolf, P. Libby, F.K. Swirski, C.S. Robbins, W. McPheat, S. Hawley, M. Braddock, R. Gilsbach, L. Hein, C. von zur Muhlen, C. Bode, A. Zirlik, I. Hilgendorf, Atheroprotection through SYK inhibition fails in established disease when local macrophage proliferation dominates lesion progression, Basic Res. Cardiol. 111 (2016), http://dx.doi.org/10.1007/s00395-016-0535-8 (20–016–0535–8. Epub 2016 Feb 18).
[74] R. Duncan, The dawning era of polymer therapeutics, Nat. Rev. Drug Discov. 2 (2003) 347–360, http://dx.doi.org/10.1038/nrd1088.
[75] B. Rihova, M. Bilej, V. Vetvicka, K. Ulbrich, J. Strohalm, J. Kopecek, R. Duncan, Biocompatibility of N-(2-hydroxypropyl) methacrylamide copolymers containing adriamycin. Immunogenicity, and effect on haematopoietic stem cells in bone marrow in vivo and mouse splenocytes and human peripheral blood lymphocytes in vitro, Biomaterials 10 (1989) 335–342 http://www.ncbi.nlm.nih.gov/pubmed/2765631 (accessed June 20, 2017).
[76] B. Říhová, K. Kubácková, Clinical implications of N-(2-hydroxypropyl)methacrylamide copolymers, Curr. Pharm. Biotechnol. 4 (2003) 311–322 http://www.ncbi.nlm.nih.gov/pubmed/14529421 (accessed June 20, 2017).
[77] R. Duncan, M.J. Vicent, Do HPMA copolymer conjugates have a future as clinically useful nanomedicines? A critical overview of current status and future opportunities? Adv. Drug Deliv. Rev. 62 (2010) 272–282, http://dx.doi.org/10.1016/j.addr.2009.12.005.
[78] J.I. Hare, T. Lammers, M.B. Ashford, S. Puri, G. Storm, S.T. Barry, Challenges and strategies in anti-cancer nanomedicine development: an industry perspective, Adv. Drug Deliv. Rev. 108 (2017) 25–38, http://dx.doi.org/10.1016/j.addr.2016.04.025.